Casimir-Polder interaction between an atom and a dielectric grating

Ana M. Contreras-Reyes,[1] Romain Guérout,[2] Paulo A. Maia Neto,[1]
Diego A. R. Dalvit,[3] Astrid Lambrecht,[2] and Serge Reynaud[2]

[1]*Instituto de Fisica, UFRJ, CP 68528, Rio de Janeiro, RJ, 21941-972, Brazil*
[2]*Laboratoire Kastler Brossel, case 74, CNRS, ENS, UPMC, Campus Jussieu, F-75252 Paris Cedex 05, France*
[3]*Theoretical Division, Los Alamos National Laboratory, Los Alamos, NM 87545, USA*

(Dated: November 24, 2010)

We develop the scattering approach to calculate the exact dispersive Casimir-Polder potential between a ground-state atom and a rectangular grating. Our formalism allows, in principle, for arbitrary values of the grating amplitude and period, and of the atom-grating distance. We compute numerically the potential for a Rb atom on top of a Si grating and compare the results with the potential for a flat surface taken at the local atom-surface distance (proximity force approximation). Except for very short separation distances, the potential is nearly sinusoidal along the direction transverse to the grooves.

I. INTRODUCTION

Vacuum field fluctuations are modified close to material surfaces, resulting in the usually attractive Casimir-Polder force [1] on a nearby ground-state atom. This effect has been measured by a number of experimental techniques, including deflection of atomic beams [2], classical [3, 4] and quantum reflection by the attractive Casimir-Polder potential [5–7], and dipole oscillations of a Bose-Einstein condensate (BEC) close to a dielectric surface [8].

More recently, experiments involving non-trivial geometries paved the way to new applications. The measured reflection probability of a BEC from a Si surface with a square array of closely spaced thin pillars increased by a factor of nearly four as compared to a flat surface [9]. A Si surface with an array of wall-like parallel ridges was shown to work as a reflection diffraction grating for atoms incident along a nearly grazing direction [10]. Several diffraction orders in the quantum reflection from a microstructured grating consisting of Cr strips on a flat quartz substrate were measured [11]. Alternatively, nano-fabricated transmission atom gratings allow for a direct measurement of the dispersive atom-surface potential in the non-retarded van der Waals regime [12].

Remarkable experimental progress has also been achieved in the closely related field of Casimir interactions between material surfaces [13]. Recent experiments have revealed interesting geometry effects in the normal force between a Si rectangular (lamellar) grating and a metallic spherical surface [14, 15] and in the lateral force between two metallic gratings [16].

This ensemble of new experiments clearly motivates the theoretical analysis of how geometry molds the quantum field fluctuations giving rise to the Casimir-Polder and Casimir interactions. In this paper, we develop a non-perturbative theory for the Casimir-Polder interaction between a ground state atom and a dielectric grating. Our results are valid, in principle, for arbitrary values of the grating amplitude. Preliminary results were already applied in the analysis of quantum vortex generation in a BEC induced by the Casimir-Polder potential of a rotating grating [17]. Here we present a detailed derivation of the Casimir-Poder potential and a variety of numerical examples that illustrate its main characteristics.

Calculations beyond the simple planar geometry are extremely involved because different frequency and length scales contribute to the interaction. Since dispersive forces are not additive, it is not possible to build up the atom-surface potential from the more elementary atom-atom interaction. In the pairwise summation (PWS) approach, the non-additivity is corrected by a 'calibration' provided by the planar case at a given separation distance range [18]. Since the non-additivity correction is geometry and distance dependent, PWS results are barely more accurate [19] than the results obtained by taking the proximity force approximation (PFA) [20], in which the potential is simply approximated by the planar case taken at the local atom-surface distance.

Only recently new theoretical tools have been developed for analyzing non-trivial geometries [21] beyond the PFA and PWS approaches. In the scattering approach [22, 23], the interaction potential is written in terms of reflection operators describing non-specular scattering (diffraction) by non-planar surfaces. This allows for a description of the Casimir effect that captures its full geometry dependence. In the specific case of the Casimir-Polder interaction between a ground-state atom and a material surface, the exact potential can be calculated for arbitrary distances, taking due account of finite response times of both atom and material medium, provided the surface reflection operator is known [24].

By computing the reflection operator of the grating as a perturbation of the planar symmetry, Refs. [24, 25] derived the Casimir-Polder potential to first order in the grating amplitude. The resulting expressions are valid only when the grating amplitude is the smallest length scale in the problem. However, in order to enhance the non-trivial geometry effects associated with the departure from the planar symmetry, it is of course interesting

to have large amplitudes. This was indeed the case in the atom-surface [9, 10] and surface-surface [14, 16] experiments carried out so far. In this paper, we compute the exact reflection operator by applying the differential theory of diffraction gratings [26], and then deriving the exact Casimir-Polder potential from the scattering approach [24]. Our approach is similar to the theory developed in Refs. [27–29] for treating surface-surface interactions.

Non-perturbative results were previously obtained for a toy model describing the Casimir interaction of a scalar field satisfying ideal Dirichlet boundary conditions with a small sphere above a corrugated surface [30]. In this paper, we develop a full electromagnetic theory that takes into account the electromagnetic responses of real atoms and material surfaces (we consider a Rb atom above a Si grating in the numerical examples). This allows us to cover the entire range of separation distances, from the unretarded short-distance van der Waals regime to the Casimir-Polder large-distance asymptotic limit.

The paper is organized as follows. In Sec. II, we derive the formal results for the Casimir energy which are applied in the numerical implementations discussed in Sec. III. Sec. IV presents our concluding remarks.

II. SCATTERING APPROACH TO THE ATOM-GRATING INTERACTION

We consider a spherically symmetric ground-state atom located at (x_A, y_A, z_A) above a non-planar surface (see Fig. 1), corresponding to a profile function $h(x, y)$ giving the local surface height with respect to a reference plane at $z = 0$. It is convenient to develop the scattering formula in the plane-wave basis $|\mathbf{k}, \pm, p\rangle$ [22], where $\mathbf{k}$ is the two-dimensional wave-vector component parallel to the xy plane, $+(-)$ represents upward (downward) propagation direction and p stands for polarization. We assume that the atom-surface separation distance $z_A - h(x_A, y_A)$ is much larger than the atomic dimensions, allowing us to approximate the potential to first order in the atomic polarizability $\alpha(\omega)$ or, equivalently, to first order in the atomic reflection operator [24]

$$\langle \mathbf{k}, -, p|\mathcal{R}_A(i\xi)|\mathbf{k}', +, p'\rangle = -\frac{\xi^2}{2\kappa}\frac{\alpha(i\xi)}{\epsilon_o c^2} e^{i(\mathbf{k}-\mathbf{k}')\cdot\mathbf{r}_A} e^{-(\kappa+\kappa')z_A}\hat{\boldsymbol{\epsilon}}_p^-(\mathbf{k}, i\xi)\cdot\hat{\boldsymbol{\epsilon}}_{p'}^+(\mathbf{k}', i\xi'), \tag{1}$$

with $\mathbf{r}_A = (x_A, y_A)$ and $\kappa = \sqrt{k^2 + \xi^2/c^2}$ representing the wave-vector z-component associated with the imaginary frequency ξ (κ' is defined in terms of $\mathbf{k}'$ in the same way). $\hat{\boldsymbol{\epsilon}}_p^{\pm}(\mathbf{k}, i\xi)$ are unit vectors corresponding to a given polarization basis (to be chosen later in this section).

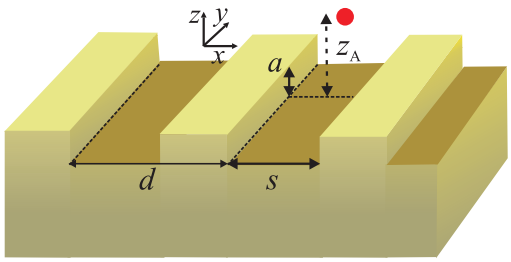

FIG. 1: Atom on top of a rectangular grating.

The zero-temperature Casimir energy is then obtained by expanding the general scattering formula [22, 23] to first order in $\mathcal{R}_A$. This corresponds to neglecting all multiple reflections between the atom and the surface (reflection operator $\mathcal{R}_S$) but the single round-trip containing one reflection by each one (see Ref. [24] for a detailed derivation). The Casimir potential is then written as an integral over the positive imaginary semi-axis in the complex frequency plane:

$$U(x_A, y_A, z_A) = -\hbar\int_0^\infty \frac{\mathrm{d}\xi}{2\pi}\int\frac{\mathrm{d}^2\mathbf{k}}{(2\pi)^2}\int\frac{\mathrm{d}^2\mathbf{k}'}{(2\pi)^2}\sum_{p,p'}\langle \mathbf{k}, +, p|\mathcal{R}_S(i\xi)|\mathbf{k}', -, p'\rangle\langle \mathbf{k}', -, p'|\mathcal{R}_A(i\xi)|\mathbf{k}, +, p\rangle. \tag{2}$$

An exact expression for the Casimir-Polder interaction energy between a ground-state atom and a generic surface can also be written in terms of an integral over real

frequencies. Once such an integral is computed with an appropriate choice of integration contour in the complex frequency plane, one recovers Eq. (2), which is in terms of purely imaginary frequencies $\omega = i\xi$. On one hand, the real frequency formalism suffers from highly oscillatory contributions, but allows for the identification of the relevant modes (evanescent and propagating) of the electromagnetic field that contribute to the interaction energy. For example, both modes are known to play a fundamental role in the Casimir energy in the plane-plane geometry [31]. We expect that both kinds of modes also have a key role in the Casimir-Polder atom-grating interaction (this analysis is beyond the scope of the present paper). On the other hand, the formalism in terms of purely imaginary frequencies has a smooth, exponentially decaying frequency behavior, but it does not allow for the identification of the separate contributions from evanescent and propagating modes. However, Eq. (2) does include the total contribution of all modes.

In this paper, we calculate the exact surface reflection operator $\mathcal{R}_S$ for the rectangular (lamellar) grating shown in Fig. 1. The periodic profile function $h(x)$ has period d, amplitude a and corresponds to a groove width s. The reference plane $z = 0$ is located at the bottom of the groove. Translational symmetry along the y direction implies that $\mathcal{R}_S$ does not change k_y. When defining the polarization basis, we exploit this symmetry as in waveguide theory: polarization H is such that $E_y \equiv 0$ with E_x, E_z, H_x and H_z given in terms of H_y by using Maxwell equations. For the electric field components at a real frequency ω propagating in a medium of dielectric constant ϵ, we have $E_x^{\mathrm{H}} = -ic\omega\partial_z H_y/(\epsilon\omega^2 - c^2k_y^2)$ and $E_z^{\mathrm{H}} = ic\omega\partial_x H_y/(\epsilon\omega^2 - c^2k_y^2)$. In vacuum ($\epsilon = 1$), the corresponding unit vectors are then given by

$$\hat{\boldsymbol{\epsilon}}_{\mathrm{H}}^{\pm}(\mathbf{k},\omega) = \frac{1}{\sqrt{\omega^2/c^2 - k_y^2}}(\mp\sqrt{\omega^2/c^2 - k^2}\,\hat{\mathbf{x}} + k_x\,\hat{\mathbf{z}}). \quad (3)$$

Polarization E is likewise defined by the condition $H_y \equiv 0$, with $E_x^{\mathrm{E}} = ic^2k_y\partial_x E_y/(\epsilon\omega^2 - c^2k_y^2)$ and $E_z^{\mathrm{E}} = ic^2k_y\partial_z H_y/(\epsilon\omega^2 - c^2k_y^2)$, so that the corresponding unit vectors are given by

$$\begin{aligned}\hat{\boldsymbol{\epsilon}}_{\mathrm{E}}^{\pm}(\mathbf{k},\omega) \;=\; \frac{c}{\omega}\Bigg[&\frac{k_y}{\sqrt{\omega^2/c^2 - k_y^2}}\left(-k_x\,\hat{\mathbf{x}} \mp \sqrt{\omega^2/c^2 - k^2}\,\hat{\mathbf{z}}\right)\\ &+\sqrt{\omega^2/c^2 - k_y^2}\,\hat{\mathbf{y}}\Bigg]. \end{aligned} \quad (4)$$

Since the surface profile is periodic along the x direction, the fields are pseudo-periodic functions of x (Bloch's theorem): $\mathbf{E}(x+d,y,z) = e^{ik_x^{(0)}d}\mathbf{E}(x,y,z)$ for some $k_x^{(0)}$ in the first Brillouin zone $[-\pi/d, \pi/d]$. The wave-vector x-component of a given incident plane wave can always be cast in the form

$$k_x^{(j)} = k_x^{(0)} + j\,\frac{2\pi}{d} \quad (5)$$

for some integer j and $k_x^{(0)} \in [-\pi/d, \pi/d]$. Diffraction by the periodic grating will give rise to new Fourier components modulated by integer multiples of $2\pi/d$. Although these new Fourier components correspond to different integers j' (with $j' - j$ representing a given diffraction order), they all correspond to the the same $k_x^{(0)}$ in the first Brillouin zone according to Bloch's theorem. For a given incident plane wave $|(k_x^{(0)} + j\,\frac{2\pi}{d})\hat{\mathbf{x}} + k_y\hat{\mathbf{y}}, -, p\rangle$, we add, in the homogenous region above the grating ($z \geq a$), a superposition of reflected plane waves $|(k_x^{(0)} + j'\,\frac{2\pi}{d})\hat{\mathbf{x}} + k_y\hat{\mathbf{y}}, +, p'\rangle$ (Rayleigh expansion), with amplitudes given by the matrix elements $\langle j', p'|\mathcal{R}_S|j, p\rangle$ of the grating reflection operator. In the bulk region $z < 0$, the dielectric constant is also uniform and the field is written as a simple plane wave expansion in terms of transmission amplitudes. On the other hand, within the inhomogeneous grating region $0 \leq z \leq a$, we derive the non-trivial z dependence of the field by solving coupled differential equations (differential approach) [26]. We then solve for the matrix elements $\langle j', p'|\mathcal{R}_S|j, p\rangle$ by matching the different field expansions at $z = a$ and $z = 0$.

The properties of the reflection operator $\mathcal{R}_S$ discussed above allow us to simplify the general expression (2) for the Casimir-Polder potential energy. By plugging the result (1) for the atomic reflection operator into (2), we find

$$\begin{aligned} U(x_A, z_A) = {}& \frac{\hbar}{\epsilon_o c^2}\int_0^\infty \frac{\mathrm{d}\xi}{2\pi}\int_{-\infty}^{\infty}\frac{\mathrm{d}k_y}{2\pi}\int_{-\pi/d}^{\pi/d}\frac{\mathrm{d}k_x^{(0)}}{2\pi}\\ &\times\sum_{j,j'}\frac{\xi^2}{2\kappa_{j'}}\alpha(i\xi)\,e^{2\pi i(j-j')x_A/d}\,e^{-(\kappa_j+\kappa_{j'})z_A}\\ &\times\sum_{p,p'}\langle j,p|\mathcal{R}_S(k_x^{(0)},k_y,i\xi)|j',p'\rangle\;\hat{\boldsymbol{\epsilon}}_p^{+}\cdot\hat{\boldsymbol{\epsilon}}_{p'}^{-\prime}. \end{aligned} \quad (6)$$

The sums over the Brillouin zones j and j' run from $-\infty$ to ∞, the polarizations p, p' are either E or H and $\kappa_j = \sqrt{k_x^{(j)2} + k_y^2 + \xi^2/c^2}$ [see Eq. (5)]. The scalar products are calculated from the expression for the unit vectors given by Eqs. (3) and (4). When replacing $\omega \to i\xi$, $\sqrt{\omega^2/c^2 - k^2} \to i\kappa_j$, we find

$$\begin{aligned}\hat{\boldsymbol{\epsilon}}_{\mathrm{H}}^{+}\cdot\hat{\boldsymbol{\epsilon}}_{\mathrm{H}}^{-\prime} \;&=\; -\frac{k_x^{(j)}k_x^{(j')} + \kappa_j\kappa_{j'}}{\xi^2/c^2 + k_y^2},\\ \hat{\boldsymbol{\epsilon}}_{\mathrm{E}}^{+}\cdot\hat{\boldsymbol{\epsilon}}_{\mathrm{E}}^{-\prime} \;&=\; 1 + \frac{c^2k_y^2}{\xi^2}\left(1 - \hat{\boldsymbol{\epsilon}}_{\mathrm{H}}^{+}\cdot\hat{\boldsymbol{\epsilon}}_{\mathrm{H}}^{-\prime}\right),\\ \hat{\boldsymbol{\epsilon}}_{\mathrm{E}}^{+}\cdot\hat{\boldsymbol{\epsilon}}_{\mathrm{H}}^{-\prime} \;&=\; -\hat{\boldsymbol{\epsilon}}_{\mathrm{H}}^{+}\cdot\hat{\boldsymbol{\epsilon}}_{\mathrm{E}}^{-\prime} = \frac{c^3k_y(k_x^{(j')}\kappa_j + k_x^{(j)}\kappa_{j'})}{\xi(\xi^2 + c^2k_y^2)}. \end{aligned}$$

The potential (6) does not depend on y_A and is a periodic function of x_A (with the same period of the grating) as expected. By choosing the origin $x = 0$ at the mid-point of one of the grooves, the matrix elements $\langle j', p'|\mathcal{R}_S|j, p\rangle$ turn out to be real and consistent with the even parity of the surface profile. They

must also satisfy reciprocity relations [32] which read, for our polarization basis, $\kappa_j\langle j,p|\mathcal{R}_S(k_x^{(0)},k_y,i\xi)|j',p'\rangle = (2\delta_{pp'}-1)\kappa_{j'}\langle -j',p'|\mathcal{R}_S(-k_x^{(0)},-k_y,i\xi)|-j,p\rangle$. By combining these properties, we may cast (6) as $U(x_A,z_A) = \sum_{j,j'} C_{j,j'}(z_A)\, e^{2\pi i(j-j')x_A/d}$ in terms of real coefficients satisfying $C_{j,j'}(z_A) = C_{j',j}(z_A)$. Thus, Eq. (6) yields a real potential satisfying the required relations $U(x_A,z_A) = U(-x_A,z_A) = U(d-x_A,z_A)$ (reflection symmetries with respect to the groove and plateau midpoints).

III. NUMERICAL RESULTS

In this section, we present numerical results for the Casimir-Polder potential given by (6). We consider a Rb atom, whose dynamic polarizability $\alpha(i\xi)$ is obtained from Ref. [33], interacting with an intrinsic silicon grating. The corresponding dielectric constant $\epsilon(i\xi)$, required for the evaluation of the grating reflection operator $\mathcal{R}_S$, is computed from available data at real frequencies [34] by using a Kramers-Kronig relation [35].

When evaluating (6), we need to truncate the sum over the Brillouin zones j,j' at some finite value $N_{\max}$, so that the number of zones is $2N_{\max}+1$. The value of $N_{\max}$ required for a given accuracy decreases with increasing distance z_A, because the factor $e^{-(\kappa_j+\kappa_{j'})z_A}$ kills the contribution of large values of j and j'. By comparing results obtained from different values of $N_{\max}$, we found that $N_{\max} = 3$ was sufficient to achieve an accuracy at the level of a percent for the numerical examples considered below.

It is instructive to compare our exact results with those obtained within the proximity force approximation (PFA) [36], which here corresponds to computing the potential U for a given surface profile from the potential $U^{(0)}$ for a planar surface taken at the local atom-surface distance: $U(x_A,y_A,z_A) \approx U^{(0)}[z_A - h(x_A,y_A)]$. For the rectangular grating considered here, deviations from PFA are quantified by the ratio $\rho = U(x_A,z_A)/U^{(0)}(z_A)$ when the atom is on top of a groove and by $\rho = U(x_A,z_A)/U^{(0)}(z_A-a)$ when the atom is on top of a plateau.

In Fig. 2, we plot ρ as a function of distance for an atom above the plateau midpoint $x_A = d/2$ and several different combinations of amplitude and period, with groove width $s = d/2$. We always find $\rho < 1$, in qualitative agreement with PWS, with the grooves making the potential less attractive than the potential of a homogeneous plane surface at $z_A = a$. When the atom is very far from the surface, $z_A \gg a$, it feels the corrugation as a very small perturbation of the plane symmetry and then the potential approaches the value for a planar surface ($\rho = 1$). As the distance decreases, the departure from the plane geometry becomes increasingly important.

The curves corresponding to the same ratio a/d are close but do not coincide, as expected since non-

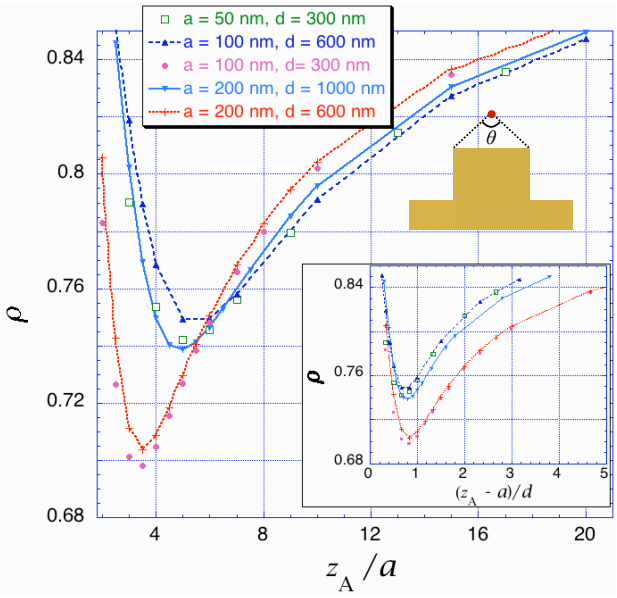

FIG. 2: Variation of $\rho = U(x_A,z_A)/U^{(0)}(z_A-a)$ versus z_A/a and $(z_A-a)/d$ (inset) for an atom above the plateau midpoint $x_A = d/2$. We take fixed values of a and d for each set of data points. The angular aperture $\theta = 2\arctan[d/4(z_A-a)]$ shown in the diagram controls the departure from the PFA limit.

geometric length scales associated to characteristic frequencies of the Rb atom and the Si bulk are also relevant. For large distances, the dominant field frequencies are much smaller than the atom and medium characteristic frequencies, and then the potential is dominated by the instantaneous response associated to the zero-frequency polarizability and dielectric constant. Thus, the potential depends only on the ratios between the geometric lengths a, d and z_A in this asymptotic limit. On the other hand, as the distance decreases, finite response times of both atom and medium give rise to a richer scenario. The crossover between the long-distance Casimir-Polder and the unretarded van der Waals regimes is in the range $200-300\,\text{nm}$ for a Rb atom interacting with a Si surface (see for instance Fig. 4 of Ref. [24]). When the separation distance decreases below $z_A/a = 5$, it already corresponds to the transition to the van der Waals regime for $a = 50\,\text{nm}$ but not yet for $a = 100\,\text{nm}$. The values for $a = 50\,\text{nm}$ then move away from the curve for $a = 100\,\text{nm}$ and the same $a/d = 1/6$ as shown in Fig. 2. A similar effect, for $a = 100\,\text{nm}, 200\,\text{nm}$ and $a/d = 1/3$ is also apparent in Fig. 2.

As ρ approaches the PFA limit $\rho \to 1$ at shorter distances, the amplitude a is no longer the most relevant length scale capturing the variation with distance. In the inset of Fig. 2, we plot ρ as a function of $(z_A-a)/d$, which is directly related to the angular aperture $\theta = 2\arctan[d/4(z_A-a)]$ of the plateau width as seen from the atom location above the plateau midpoint (see diagram in Fig. 2). When θ is very close to 180^o $[(z_A-a)/d \ll 1]$, we expect the effect of the border of the plateau to be

negligible, and then the potential should be well approximated by the result for an infinite plane (PFA). The inset of Fig. 2 shows that the variable $(z_A - a)/d$ indeed captures the main effect behind the departure from PFA as the atom is displaced away from the surface, since the curves corresponding to different values of amplitude and period collapse near each other at short distances. For all different values of a and d shown in the figure, the point of maximum $1 - \rho$ is near $(z_A - a)/d \sim 0.8$, corresponding to an angular aperture $\theta \approx 35^o$. The maximum $1 - \rho$ depends mainly on a/d and is larger for larger a/d as expected.

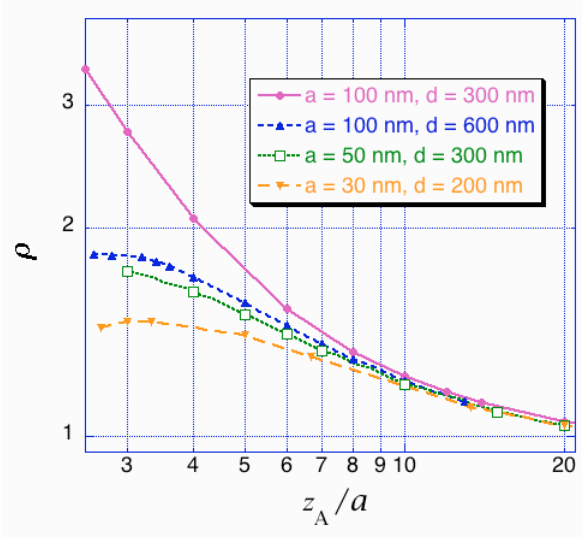

FIG. 3: Variation of $\rho = U(x_A, z_A)/U^{(0)}(z_A)$ versus z_A/a for an atom above the groove midpoint $x_A = 0$.

When the atom is above the groove region, the potential is stronger than the potential for a planar surface at the bottom of the groove ($\rho > 1$), again in qualitative agreement with the PWS picture. In Fig. 3, we plot ρ as a function of distance for $x = 0$ (groove midpoint) and $s = d/2$. The curves corresponding to different (fixed) values of a and d merge at distances $z_A/a \gtrsim 8$. This remarkable property was first found in Ref. [30] in the context of the scalar Casimir-Polder model. It may be interpreted as an effect of averaging the small length scales associated to the surface profile when considering the long-wavelength field fluctuations that provide the main contribution at large distances.

At shorter distances, the curves move apart following the order of larger a/d. Although atomic/material frequency scales play a relevant role at $z_A < 300\,\text{nm}$, the values for different a and d with the same a/d shown in Fig. 3 are still relatively close.

From an overall comparison of Figs. 2 and 3, we may conclude that the relative deviation from PFA $|\rho - 1|$ is generally larger above the groove than above the plateau. In Fig. 4, we plot $|\rho - 1|$ as a function of the lateral position for a fixed local distance $z_A - h(x_A) = 3a$, with

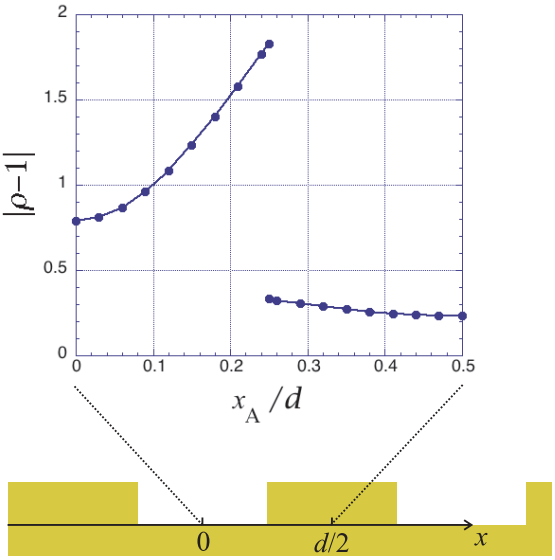

FIG. 4: Lateral variation of $|\rho - 1|$ at a fixed local distance $z_A - h(x_A)$ with $a = 100\,\text{nm}$ and $d = 600\,\text{nm}$. We take $z_A = 3a$ above the groove ($0 \le x_A < d/2$), and $z_A = 4a$ above the plateau ($d/2 \le x_A < d$).

$a = 100\,\text{nm}$, $d = 600\,\text{nm}$, and $s = 300\,\text{nm}$. PFA is indeed worse above the groove, where the deviation increases rapidly as one approaches the corner. Above the plateau, PFA is also worse near the corner, but the variation of ρ with lateral position is much smaller.

At a given plane $z = z_A$, the potential profile along the x axis is approximately sinusoidal for the relatively large distances considered here. In Fig. 5a, we compare the values for $U(x_A, z_A)/U^{(0)}(z_A - a/2)$ with a sinusoidal variation (solid line) corresponding to period d and amplitude $[U(d/2, z_A) - U(0, z_A)]/2$. We use $z_A = 3a$ and the same parameters employed in Fig. 4.

At very large distances, the main contribution comes from specular reflection at the first Brillouin zone $j = j' = 0$, yielding a flat potential according to Eq. (6) (see Figs. 2 and 3). As the distance decreases, the major correction, corresponding to the first diffraction order $j - j' = \pm 1$, produces a sinusoidal modulation with period d. Deviation from the sinusoidal shape (coming from $|j - j'| \ge 2$) is such that the lateral force stiffness $|\partial^2 U/\partial x_A^2|$ is slightly larger at the groove midpoint than at the plateau midpoint, as shown in Fig. 5a.

The deviation from the sinusoidal shape and the amplitude of oscillation are controlled by the angular aperture parameter $(z_A - a)/d$, whereas z_A/a controls the convergence of the spatial average $\langle U(x_A, z_A)\rangle$ to its large distance limit $U^{(0)}(z_A - a/2) = [U^{(0)}(z_A - a) + U^{(0)}(z_A)]/2 + \mathcal{O}(a/z_A)^2$ when $s = d/2$. For instance, in Fig. 5b we plot the potential as a function of x_A/d for $z_A = d = 2a = 200\,\text{nm}$. These parameters correspond to $z_A/a = 2$ and $(z_A - a)/d = 0.5$, to be compared with $z_A/a = 3$ and $(z_A - a)/d = 0.33$ for Fig. 5a. While the average potential is closer to the asymptotic value

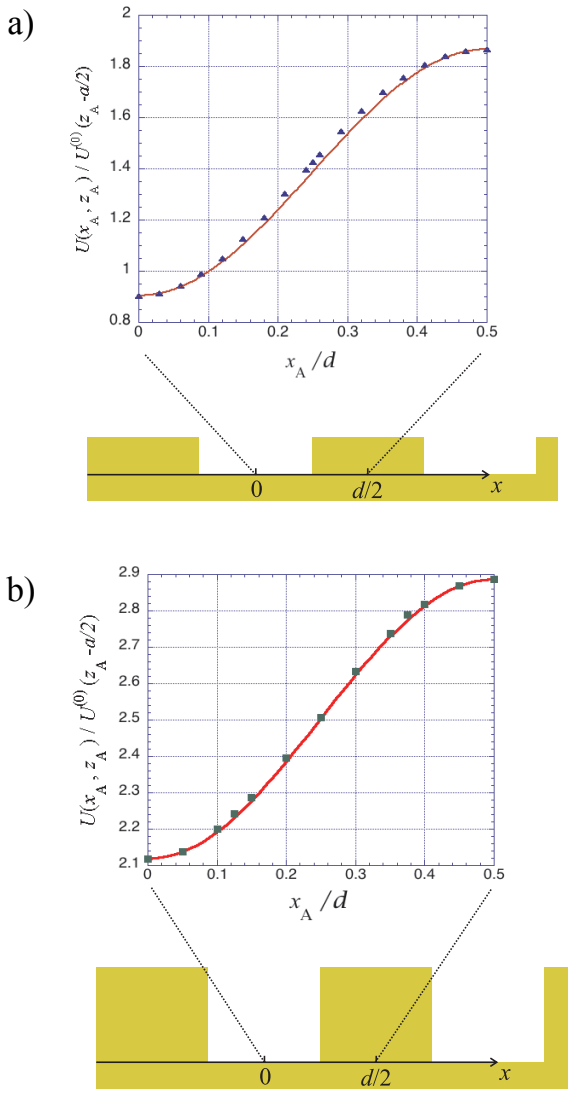

FIG. 5: Lateral variation of the Casimir-Polder potential divided by $U^{(0)}(z_A - a/2)$ for $a = 100\,\text{nm}$ with (a) $d = 2z_A = 6a$; and (b) $d = z_A = 2a$. The solid lines represent the sinusoidal function of period d that coincides with the exact potential at the groove and plateau midpoints.

$U^{(0)}(z_A - a/2)$ in Fig. 5a (larger z_A/a), the amplitude is smaller and the shape closer to the sinusoidal fit in Fig. 5b (larger $(z_A - a)/d$). As the atom is displaced away from the surface, the potential becomes more sinusoidal and with a smaller amplitude. With the same parameters of Fig. 5b, the amplitude decreases by two and three orders of magnitude at $z_A = 3a$ and $z_A = 4a$, respectively.

IV. CONCLUDING REMARKS

We have shown that PFA overestimates the potential strength above the plateau. As the atom is displaced away from surface, the deviation $1 - \rho$ is mainly controlled by the parameter $(z_A - a)/d$ associated to the angular aperture of the plateau as seen by the atom. The maximum deviation takes place near $(z_A - a)/d = 0.8$ and is larger for deeper grooves (larger a/d) as expected. As the distance is increased past this value, the potential again approaches the result for a planar surface. On the other hand, the potential is underestimated by the PFA above the groove. The deviation increases strongly as the atom is laterally displaced closer to a corner, where the presence of the ridge walls have a stronger effect.

The naive PWS picture of the Casimir-Polder interaction agrees qualitatively with several features found in this paper. Nevertheless, PWS typically underestimates the magnitude of the Casimir-Polder potential in the grating geometry [19], particularly in the non-perturbative regime considered here [17]. For instance, it predicts an anisotropy of the Casimir-Polder potential far too small to nucleate vortices in a Bose-Einstein condensate by rotation of the grating, whereas the exact theory presented here predicts an anisotropy above the required values under realistic experimental conditions [17].

We have shown that the contribution of higher diffraction orders to the potential is increasingly small as the distance increases, resulting in a sinusoidal variation along the transverse x direction for $(z_A - a)/d \gtrsim 0.5$ (aperture angle smaller than 53^o).

The scattering approach developed in this paper might be readily adapted to consider more general two-dimensional periodic patterns, like the pillars structure employed in the quantum reflection experiment reported by Ref. [9]. Recently, the Casimir interaction between two material surfaces imprinted with two-dimensional periodic patterns has been analyzed in detail [37]. The method developed here thus paves the way for the quantitative analysis of a variety of interesting geometries with applications in enhanced atomic quantum reflection and diffraction.

Acknowledgments

We would like to thank François Impens and Valery Marachevsky for discussions. This work was partially supported by CAPES-COFECUB, CNPq, DARPA, ESF Research Networking Programme CASIMIR and FAPERJ-CNE.

[1] H. Casimir and D. Polder, Phys. Rev. **73**, 360 (1948).
[2] C. I. Sukenik, M. G. Boshier, D. Cho, V. Sandoghdar, and E. A. Hinds, Phys. Rev. Lett. **70**, 560 (1993).
[3] A. Landragin, J. Y. Courtois, G. Labeyrie, N. Vansteenkiste, C. I. Westbrook, and A. Aspect, Phys. Rev. Lett. **77**, 1464 (1996).

[4] H. Bender, Ph. W. Courteille, C. Marzok, C. Zimmermann, and S. Slama, Phys. Rev. Lett. **104**, 083201 (2010).

[5] F. Shimizu, Phys. Rev. Lett. **86**, 987 (2001).

[6] V. Druzhinina and M. DeKieviet, Phys. Rev. Lett. **91**, 193202 (2003).

[7] T. A. Pasquini, Y. Shin, C. Sanner, M. Saba, A. Schirotzek, D. E. Pritchard, and W. Ketterle, Phys. Rev. Lett. **93**, 223201 (2004).

[8] D. M. Harber, J. M. Obrecht, J. M. McGuirk, and E. A. Cornell, Phys. Rev. A **72**, 033610 (2005); J. M. Obrecht, R. J. Wild, M. Antezza, L. P. Pitaevskii, S. Stringari, and E. A. Cornell, Phys. Rev. Lett. **98**, 063201 (2007).

[9] T. A. Pasquini, M. Saba, G.-B. Jo, Y. Shin, W. Ketterle, D. E. Pritchard, T. A. Savas and N. Mulders, Phys. Rev. Lett. **97**, 093201 (2006).

[10] H. Oberst, D. Kouznetsov, K. Shimizu, J. I. Fujita and F. Shimizu, Phys. Rev. Lett. **94**, 013203 (2005).

[11] B. S. Zhao, S. A. Schulz, S. A. Meek, G. Meijer and W. Schöllkopf, Phys. Rev. A **78**, 010902(R) (2008).

[12] J. D. Perreault, A. D. Cronin and T. A. Savas, Phys. Rev. A **71**, 053612 (2005); V. P. A. Lonij, W. F. Holmgren and A. D. Cronin, Phys. Rev. A **80**, 062904 (2009).

[13] F. Capasso, J. N. Munday, D. Iannuzzi, and H. B. Chan, IEEE J. Quantum Electron. **13**, 400 (2007).

[14] H. B. Chan, Y. Bao, J. Zou, R. A. Cirelli, F. Klemens, W. M. Mansfield, and C. S. Pai, Phys. Rev. Lett. **101**, 030401 (2008).

[15] Y. Bao, R. Guérout, J. Lussange, A. Lambrecht, R. A. Cirelli, F. Klemens, W. M. Mansfield, C. S. Pai and H. B. Chan, e-print arXiv:1009.3487 (2010).

[16] H.-C. Chiu, G. L. Klimchitskaya, V. N. Marachevsky, V. M. Mostepanenko and U. Mohideen, Phys. Rev. B **80**, 121402(R) (2009).

[17] F. Impens, A. M. Contreras-Reyes, P. A. Maia Neto, D. A. R. Dalvit, R. Guérout, A. Lambrecht and S. Reynaud, e-print arXiv:1007.1657 (2010).

[18] See, for instance, V. B. Bezerra, G. L. Klimchitskaya, and C. Romero, Phys. Rev. A **61**, 022115 (2000).

[19] D. A. R. Dalvit, P. A. Maia Neto, A. Lambrecht and S. Reynaud, J. Phys. A: Math. Theor. **41**, 164028 (2008)

[20] B. V. Derjaguin and I. I. Abrikosova, Sov. Phys. JETP **3**, 819 (1957); B. V. Derjaguin, Sci. Am. **203**, 47 (1960).

[21] K. Milton and J. Wagner, J. Phys. A: Math. Theor. **41**, 155402 (2008); S. J. Rahi, T. Emig, N. Graham, R. L. Jaffe, M. Kardar, Phys. Rev. D **80**, 085021 (2009); S. Reynaud, A. Canaguier-Durand, R. Messina, A. Lambrecht and P. A. Maia Neto, Int. J. Mod. Phys. A **25**, 2201 (2010).

[22] A. Lambrecht, P. A. Maia Neto and S. Reynaud, New J. Phys. **8**, 243 (2006).

[23] T. Emig, N. Graham, R. L. Jaffe, and M. Kardar, Phys. Rev. Lett. **99**, 170403 (2007).

[24] R. Messina, D. A. R. Dalvit, P. A. Maia Neto, A. Lambrecht and S. Reynaud, Phys. Rev. A **80**, 022119 (2009).

[25] D. A. R. Dalvit, P. A. Maia Neto, A. Lambrecht, and S. Reynaud , Phys. Rev. Lett **100**, 040405 (2008).

[26] M. Nevière and E. Popov, *Electromagnetic theory of gratings: review and potential applications*, in Proc. SPIE, W. R. McKinney and C. A. Palmer (eds.), Vol. 3450, pp. 2-10 (1998).

[27] A. Lambrecht and V. N. Marachevsky, Phys. Rev. Lett. **101**, 160403 (2008).

[28] H.-C. Chiu, G. L. Klimchitskaya, V. N. Marachevsky, V. M. Mostepanenko and U. Mohideen, Phys. Rev. B **81**, 115417 (2010).

[29] A. Lambrecht, A. Canaguier-Durand, R. Guérout and S. Reynaud, e-print arXiv:1006.2959 (2010).

[30] B. Döbrich, M. DeKieviet and H. Gies, Phys. Rev. D **78**, 125022 (2008).

[31] C. Henkel, K. Joulain, J.-Ph. Mulet, and J.-J. Greffet, Phys. Rev. A **69**, 023808 (2004); F. Intravaia and A. Lambrecht, Phys. Rev. Lett. **94**, 110404 (2005); F. Intravaia, C. Henkel, and A. Lambrecht, Phys. Rev. A **76**, 033820 (2007).

[32] R. Carminati, M. Nieto-Vesperinas and J.-J. Greffet, J. Opt. Soc. Am. A **15**, 706 (1998).

[33] A. Derevianko, S. G. Porsev and J. F. Babb, At. Data Nucl. Data Tables **96**, 323 (2010).

[34] Handbook of Optical Constants of Solids, edited by E. Palik (Academic Press, New York, 1998).

[35] A. Lambrecht and S. Reynaud, Eur. Phys. J. D **8**, 309 (2000).

[36] B. V. Deriagin, I. I. Abrikosova, and E. M. Lifshitz, Quart. Rev. **10**, 295 (1968).

[37] P. S. Davids, F. Intravaia, F. S. S. Rosa and D. A. R. Dalvit, e-print arXiv:1008.3580 (2010).